Facing death: a multidisciplinary analysis of a Romano-Egyptian mummy mask at the Ny Carlsberg Glyptotek, Copenhagen

Tuuli Kasso[1,2*], Jens Stenger[2], Caterina Zaggia[3], Gianluca Pastorelli[4], Max Ramsøe[1], Tina Ravnsborg[5], Ole N. Jensen[5], Elsa Yvanez[6], Chiara Spinazzi-Lucchesi[6], Matthew J. Collins[1,3] and Cecilie Brøns[2]

Abstract

Funerary masks played a crucial role in ancient Egyptian burial practices, as part of the rituals to ensure a successful afterlife. This study presents the first comprehensive analysis of a gilded mummy mask from the Roman period in Egypt from the collections of The Ny Carlsberg Glyptotek in Copenhagen. Portraying a young female, the mask belongs to a distinctive group of mummy masks, whose origins can be identified to be coming from the Dakhlah and Kharga oases. The construction of the mask (plaster, textiles) and the constituents of its polychromy (pigments, binding media) was analysed using various non- and micro-destructive methods: imaging, cross-section analysis, optical microscopy, Fourier transform infrared spectroscopy and scanning electron microscopy coupled to energy-dispersive X-ray spectroscopy. Additionally, samples were taken for palaeoproteomic analysis with liquid chromatography–tandem mass spectrometry. A wide range of pigments such as yellow and red ochre, carbon-based black, and Egyptian blue were identified, reflecting common materials in polychromy in Egypt during the Roman period. Notably, indigo was detected, suggesting its usage in mixtures to render purple hues. Analysis of adhesives and media identified plant gum and collagen-based animal glue. Proteomic analysis identified *Equus asinus* (donkey) as the predominant protein source for the collagen-based glue. The results shed light on the materials and techniques employed in ancient polychromy in Egypt in the Roman period, further enriching our understanding of artistic practices at the time.

Keywords Ancient Egypt, Mummy masks, Material analysis, Polychromy, Inorganic analysis, Palaeoproteomics

*Correspondence:
Tuuli Kasso
tuuli@palaeome.org
[1] Globe Institute, University of Copenhagen, Øster Farimagsgade 5, 1353 Copenhagen, Denmark
[2] Ny Carlsberg Glyptotek, Dantes Plads 7, 1556 Copenhagen, Denmark
[3] The McDonald Institute for Archaeological Research, University of Cambridge, Downing St., Cambridge CB2 3ER, UK
[4] National Gallery of Denmark (Statens Museum for Kunst, SMK), Sølvgade 48-50, 1307 Copenhagen, Denmark
[5] Department of Biochemistry and Molecular Biology, University of Southern Denmark, 5230 Odense, Denmark
[6] Centre for Textile Research, Saxo Institute, University of Copenhagen, Karen Blixens Plads 8, 2300 Copenhagen, Denmark

Introduction

In ancient Egypt, proper treatment of the body was an important part of the burial ensuring a successful afterlife. The burial also often included a stylized portrait in the form of a mummy mask that covered the face and upper body of the deceased [1–3]. Intricate mummy masks were available for the elite [4], as the costly materials made it an art form beyond the financial reach of most citizens [5, 6].

Mummy masks were manufactured in various ways and styles as the Egyptian funerary rites developed [1, 3]. They were typically made in cartonnage (cloth fortified with plaster and glue), which was widely used for masks from the Middle Kingdom (2040–1786 BCE) onwards

[1–3]. Often gilding was applied to the faces of the masks, a tradition which continued until mummification receded from the funerary traditions around the fourth century CE [5–7].

Different traditions of funerary art existed during the Roman period in Egyptian period, including mummy portraits painted on wood, three-dimensional mummy busts in gypsum, and cartonnage mummy masks [5, 8]. These three distinct artistic styles point towards diversity and rich cultural influences during the Roman period in Egypt. Mummy and funerary portraits painted on wood have been extensively researched [1, 2, 9–13]. Pre-Roman gilded mummy masks have also been the focus of multiple studies [3, 14–18]. Except for a few recent studies [19, 20], gilded mummy masks from the Roman period in Egypt are an understudied group and no extensive material analysis has yet been conducted on this type of artefact.

The primary objective of the present study is to investigate the materials and techniques employed in the production of a gilded mummy mask (ÆIN 297) from the collections of The Ny Carlsberg Glyptotek in Copenhagen. Material analysis is essential to understand the craftsmanship and production of the mask. Moreover, material analysis allows us to place it within the current knowledge of the contemporary mummy masks in the Roman period in Egypt and their makers.

The choice of materials used for an artefact is rarely a purely objective matter: The artisans need to meet their own requirements and preferences, but also those of the client. The materials used reflect the availability of materials, the methods and techniques used, and the trends of their time, but also individual choices [21]. The availability of materials may also have impacted regional craftsmanship styles, affecting the quality of their work. Furthermore, any technological information can point towards socio-economic aspects, trade networks, and artistic trends, thereby deepening our understanding of Egyptian society during the Roman period and its relationships with neighbouring cultures.

Mummy mask for a woman (ÆIN 297)
Acquisition
The mummy mask was acquired by the founder of the Ny Carlsberg Glyptotek (henceforth abbreviated as the NCG), Carl Jacobsen (1842–1914) during the end of the nineteenth century. The mask was included in the collections of the museum, which today holds a fine collection of ancient Egyptian art. During the mid-1880s, Carl Jacobsen began acquiring his first Egyptian antiquities. These acquisitions were mainly made in the international art market. In 1884, he bought the first artefact, which would lay the ground for his Egyptian collection:

a coffin with the mummified remains of a woman (ÆIN 978) [22]. In 1888 three additional coffins followed (ÆIN 302, 298, and 299), and in 1890 he acquired his first Egyptian statues at an auction in Paris. However, he desired a greater, more extensive Egyptian collection, and he therefore contacted Valdemar Schmidt (1836–1925), who Jacobsen later described as the actual creator of the museum's Egyptian collection. During the period from 1892 to 1910, Valdemar Schmidt made several acquisitions on behalf of Jacobsen on his many trips to Egypt. Moreover, Schmidt introduced Jacobsen to the British Egyptologist Sir Flinders Petrie (1853–1942), who carried out numerous excavations in Egypt from 1884 to 1926. These excavations were financed by European and American museums, which in turn received many of the finds. Jacobsen also supported these excavations, and several of the artefacts in the collections of the NCG originate from Petrie's excavations [22, 23].

Unfortunately, we do not have much specific information regarding the acquisition of the mummy mask ÆIN 297. It is recorded in the museum's inventory protocol, but the exact year when it entered the museum is unknown, as is also the name of the vendor and the price. It would appear that it was acquired on the art market in Egypt by Valdemar Schmidt sometime during the 1890s. This also means that there is no information about its findspot.

Description
The cartonnage mask is made using a mould, with layered textile as support and a layer of plaster on the surface. The mask was then painted and gilded, while the hair was made with added plant fibres. The mask is in the shape of an almost three-dimensional portrayal of a woman's upper body and face. It represents the head, chest, arms, and hands of a young woman with a gilded face. Her curly, black hair, now mostly lost, is styled as loosely hanging on both sides of her face. She is wearing a moulded, pink hairband, representing a stylized flower garland, possibly of rosebuds [24]. She is dressed in a tunic with *clavi* (vertical stripes) rendered with black, pink, and blue vertical stripes along its borders. Over this, she wears a fringed, yellow mantle or shawl with two parallel red and pink stripes or bands along its border. Her garments are stylistically rendered, not reflecting the dress as exactly worn in real life, which makes the details challenging to decipher. Both the striped *clavi* and the mantle appear on masks and coffins from other areas in Egypt, particularly on the elaborate coffins from Akhmim (for examples, see [25]; pl. 7, 31, 34).

The position of the mantle, with one end hanging freely on the breast and the other one placed horizontally, is also seen on several coffins from Akhmin, where the

Kasso *et al. Heritage Science*   (2024) 12:250

Page 3 of 22

mantles are decorated with geometric patterns.[1] Furthermore, textiles with bands made of cotton or wool are also well known from archaeological excavations in Kellis (Kharga oasis). However, here, they are mainly associated with house furnishings [26].

A triangular zigzag pattern in black adorns the area across the mask's abdomen, extending upward to the chest where it forms a knot or fold. The mantle is then wrapped around this central feature. Knots on mantles, similar to the one rendered on the mummy mask, have been associated with the cult of Isis [5]. However, they also served as a typical attribute of female iconography [20]. The zigzag motive appears, so far, as typical of a specific group of masks (see below) and is not attested elsewhere. It is difficult to understand what it is intended to represent. It could be interpreted as an evocation of the lotus flower, symbolising rebirth, or be a reminiscent nod to the bandages that traditionally form lozenge patterns on mummies since the Late Period (664–332 BCE) [5, 8]. In the latter scenario, it is distinctly a depiction of a piece of cloth, with the 'wrappings' already painted onto the fabric.

She is adorned with gilded jewellery, including a beaded necklace with a crescent-shaped pendant, termed *lunula*, an arm ring on each upper arm, a finger ring on her left ring finger, and two bracelets on her left wrist. The *lunula* pendant possibly refers to the equation of women to the goddess Hathor and her headdress of cow horns [5]. Her arms are rendered in a light skin tone. The back of the head is separated from the hair by a dotted string and decorated by a depiction of a falcon with a solar disc on its head and with the Feather of Maat at its wingtips (Fig. 1b). This central image is flanked by vertical stripes in red and green. The composition is similar to the other contemporary masks mimicking a coffin, but the details of the wreath covering part of it and the dotted decoration might suggest that it was supposed to render a veil.

Date and provenance

From the Ptolemaic period onwards, Greco-Roman influences were incorporated into the traditional Egyptian mummification rituals. This impacted the production of a variety of funerary materials such as cartonnage mummy masks, foot-cases, shrouds, and full body covers that can be characterised by the coexistence of traditional Egyptian imagery and Greco-Roman features [6, 27, 28]. Thus, the production of funerary art during this period

is as much an expression of cultural interactions as the diversity in traditions [5, 8, 29].

The mask examined in this study belongs to a distinctive group, whose origins can be identified as from the Dakhlah and Kharga oases [19] (Fig. 2). A total of 12 masks, either complete or fragmented, have been securely ascribed to this region, as they were uncovered in recent archaeological excavations [19]. Moreover, another seven masks, including the one in the NCG, are part of museum or private collections and are without their original context.[2]

The majority of these masks are associated with the oasis of Dakhla, specifically the village of Ismant al-Kharab/Kellis. According to Rindi Nuzzolo, who produced a typology of these masks based on different iconographic and stylistic details, two groups of craftsmen were active, defined as group A and B. ÆIN 297 was produced by Group A, which was the most active in Kellis. However, this group was active also in Kharga, particularly in Ain Labakha and el-Der [19]. The contact between these two oases is well-known and documented [19, 31]. While it is highly likely that the mask ÆIN 297 is connected to the necropolis of Kellis, we cannot assert this with absolute certainty, and its origin might be the necropolis of Kharga.

The group of masks, to which ÆIN 297 belongs to, has been dated to a period between the first and third centuries CE. The Kellis necropolis has been subject to many disturbances from antiquity to modern times: Family tombs were used for several decades and the site has been looted over the years, resulting in disturbed contexts, which makes stratigraphical dating of the site difficult [19]. Additionally, it has not been possible to establish a relative chronology of the typologies, since masks rendered in Ptolemaic or Roman style seem to coexist with those featuring purely Egyptian motifs, until the abandonment of the necropolis in the third century CE [19].

Conservation

The mummy mask has undergone intensive conservation. Between 1950 and 51 it was cleaned and repaired by the museum's conservator, William Larsen. In 1955, the mummy mask was taken to further conservation after damage caused by humidity. No more information is recorded in the museum's archives on the cause of the damages. The old canvas was straightened and the cracked, loose pieces of the mask were reattached by using cellulose glue. In addition, the mask was reinforced

---

[1] In some cases, as one coffin in the British Museum (BM EA29586) and a mummy cover in the National Museum of Copenhagen (inv. 5172), a woman is represented with a striped tunic with a *clavi* under the mantle.

[2] Christie's 25 November 1997 lot. n. 156; Emory University, Atlanta inv. no. 2013.43.8; Bonhams, London, 24 June 1998, lot 374; Christie's 8 April 1998 lot. n. 147; Arte Primitivo, New York, October 2008, lot 258; Sadigh Gallery, October 2013, lot 23863; The Ny Carlsberg Glyptotek ÆIN 297.

Fig. 1 **a** Front of the mummy mask. **b** Backside of the head of the mask. **c** The left side and **d** The right side of the mask. The artefact is ca. 60 cm in length, 37 cm wide and 21 cm in depth. Images by Anders Sune Berg © the Ny Carlsberg Glyptotek

with a new support on its backside with cellulose glue and fixed on a wooden board. The entire mask was then finally given a coating of an alloprene lacquer, which is a chlorinated rubber [32]. Due to the conservation of the mask, both in the sampling and data analysis process, careful consideration was given to potential conservation treatments introducing modern contamination, with

samples specifically taken from less conserved areas to ensure the integrity and accuracy of the results.

Methods
A wide range of non- and micro-destructive methods were applied for the broadest amount of information possible about the materials and techniques employed
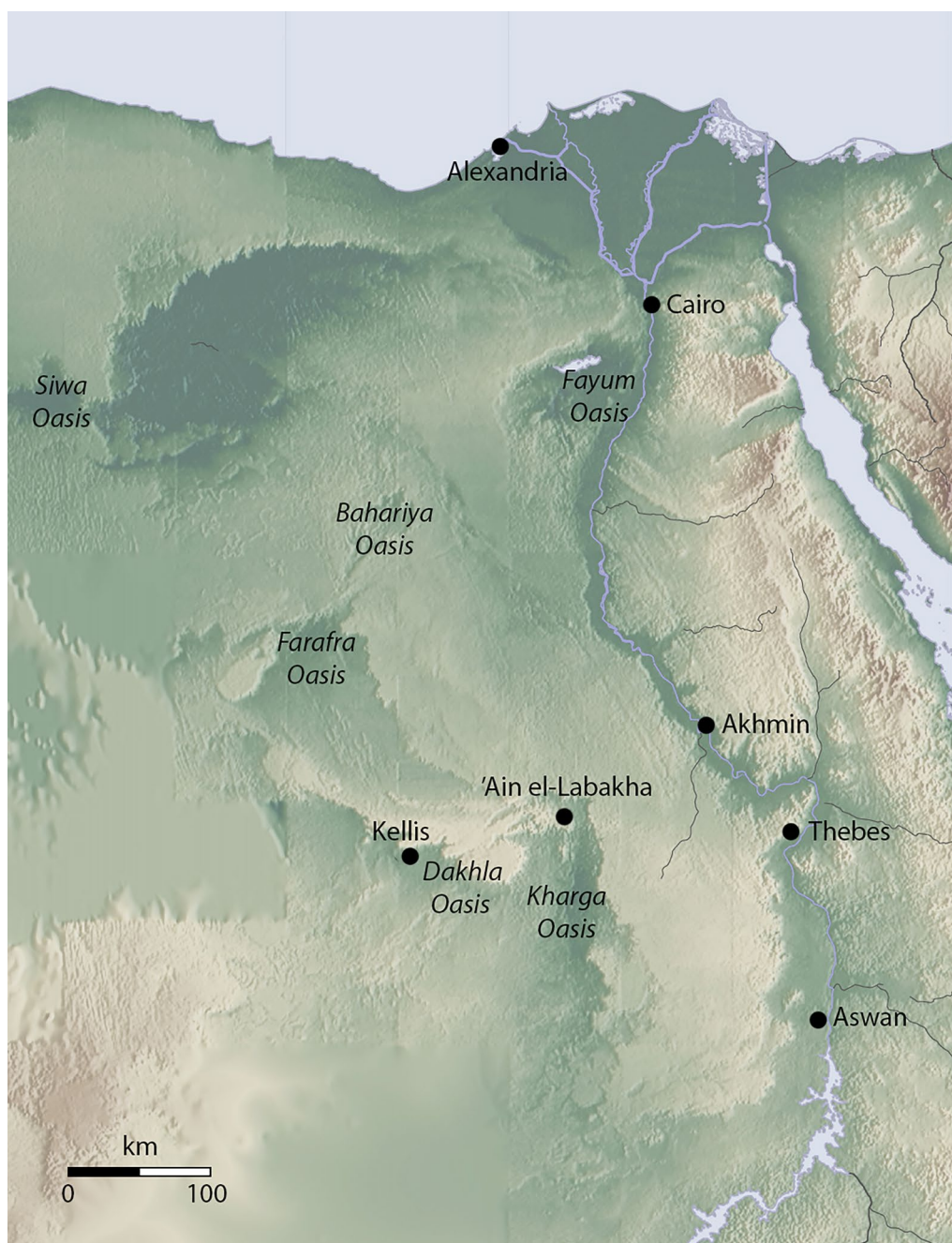
Fig. 2 Map of Egypt including the locations relevant to this study. Wikimedia Commons map (CC BY-SA 3.0 DEED). Adaptations after Rindi Nuzzolo 2023 [19] and Bagnall et al. 2016 [30]

in the production of the mummy mask. As the first step, the mask was examined visually, as a part of a condition assessment of the artefact, followed by a complete survey with technical imaging and photographic documentation. This provided the basis for the choice of analytical approaches to identify the materials and techniques used in its construction. The choice of instrumentation was also influenced by the availability and financial constraints within the timeframe of the study.

Micro samples were then taken for additional analysis of paint and adhesive compounds (FTIR, proteomics) and a cross-section was prepared for the investigation of the gilding and plaster composition with SEM–EDS.

Kasso *et al. Heritage Science*   (2024) 12:250

Page 6 of 22

Additionally, samples of the textiles and fibres were taken for further identification.

Imaging

Macroscopic imaging was performed with a modified Canon EOS 5D Mark IV camera body and an EF 50 mm f/2.5 Compact Macro lens. The filter in front of the ca. a 30.4-megapixel CMOS camera sensor was removed to extend the wavelength range into the ultraviolet (UV) and infrared (IR) spectral range.

For regular, visible light photography (VIS) including raking light imaging an X-Nite CC1 filter from MaxMax. com was used in combination with incandescent tungsten lamps. The UV-induced visible fluorescence (UVF) was recorded using X-Nite CC1, Tiffen Haze 2E, and PECA 916 filters for detection and Hoenle UVA SPOT 400/T lamps filtered with a Schott UG2A glass as excitation. Capturing the reflected UV radiation (UVR) the same UV lamps were employed and a Midwest Optical Systems BP324 filter in combination with X-Nite CC1 ensured the spectral sensitivity exclusively in the UV. Infrared reflected imaging (IRR) was performed with the tungsten lamps and a Schott RG830 filter. In the visible-light-induced infrared luminescence (VIL) imaging mode Excled LED RGB lamps (470, 525, and 629 nm) served as excitation while the camera was equipped with the same Schott RG830 filter for detection. Two narrow-band filters (Midwest Optical Systems BP635 and BP735) were used in a procedure called multiband reflectance image subtraction (MBR) by Bradley et al. [13]. The MBR image resulting from a subtraction can detect the presence of indigo but is also sensitive to other materials [33].

Textile and fibre analysis

The analysis of the textile layers that form the primary medium of the plaster surface, was carried out in situ. As ÆIN 297 is mounted on a support, it was not possible to observe it from underneath. Therefore, the textiles are only available for observation from the front, through cracks in the plaster or areas where plaster fragments have fallen off. This has complicated the use of common textile analysis tools, such as a thread counter and a hand-held digital microscope (DinoLite). Still, it was possible to record the main weave features and to obtain DinoLite pictures in several areas, allowing us to draw several conclusions on the textiles' manufacture. The thread counts, for example, were impossible to gather with a regular thread counter and were instead counted on the DinoLite photographs (extrapolated from 0.5 cm).

The previous use of conservation treatments, which seems to cover selected areas in a glue-like coating, constituted another obstacle to the study of the fibres. To address this problem, two samples were retrieved from the main break, at the front, and mounted on microscope slides to be analysed in TexLab, at the Centre for Textile Research, University of Copenhagen. The slides were examined with a Transmitted Light microscope (Leica DM750), at 4×, 10×, 40, and 63× magnification.

Fourier transform infrared spectroscopy (FTIR)

In total 16 micro samples were taken for analysis with FTIR (Fig. 8). As the samples were collected after imaging, this enabled us to avoid taking them from areas with clear presence of modern contamination from conservation treatments such as glue used in consolidation (Fig. 10), not visible to the naked eye. Each sample was taken by scraping gently with a clean scalpel, and all tools used were cleaned with ethanol between samples. Before using the instrument for measurement, the grains were carefully selected for inspection to prevent any interference from contaminants. More samples were added to the analytical process after the initial measurements, therefore two types of instrumentation were used.

Preliminary measurements were carried out with a Bruker ALPHA FTIR spectrometer equipped with a high-performance ATR accessory, a deuterated L-alanine doped triglycine sulfate (DLATGS) detector, and OPUS software version 7.8.44. ATR spectra were acquired over the range of 4000–400 cm^{-1}, with 128 scans at a resolution of 4 cm^{-1}. Some samples were prepared by flattening them onto a diamond window and subsequently analysed in transmission mode between 4000 and 600 cm^{-1} on a Thermo Scientific FTIR spectrometer coupled to a Nicolet Continuum infrared microscope (Thermo Fisher Scientific Inc., Waltham, Massachusetts, U.S.). A liquid nitrogen-cooled mercury cadmium telluride (MCT) detector recorded the signal. The resulting data and spectra were then compared with reference libraries.

Cross-section and scanning electron microscopy coupled with energy-dispersive X-ray analysis (SEM–EDS)

A sample for the cross-section was taken with the primary objective of observing the preparatory layers for gilding with an optical microscope. The sample was taken from a slightly damaged area on the right ear area of ÆIN 297 with a clean scalpel, and inspected with a microscope to ensure it was a good and intact representation of the different layers. After this, the sample was placed in an EasySection specifically designed for paint cross-section analysis (from Preservation Equipment Ltd, Norfolk, UK), embedded in resin (Technovit® 2000 by Kulzer) and cured under blue light, followed by additional days of setting at room temperature. The hardened sample was prepared as a cross-section by manually cutting and wet sanding (using a grit range of 800–4000 grains/ cm^2) the transverse plane, to ensure surface control and

Kasso *et al. Heritage Science*   (2024) 12:250

Page 7 of 22

avoid sample loss. Subsequently, mechanical polishing was conducted using grits within the range of 8000 and 12.000 grains/cm^2. The cross-section was inspected and documented with a Leica DM2500M optical microscope with 50× under reflected visible illumination using bright field (BF) and dark field (DF).

Elemental analysis on the cross-section was carried out at the scientific laboratory of the Royal Danish Academy Institute of Conservation in Copenhagen, using a Hitachi S-3400N scanning electron microscope equipped with an energy-dispersive X-ray spectrometer. The spectrometer is a Bruker Quantax 200 EDS system with two Peltier-cooled XFlash silicon drift detectors (SDD), which have an active area of 20 mm^2 each. Measurements were performed in variable pressure mode (30 Pa) on the non-coated polished section using an accelerating voltage of 20 kV, a probe current of 50 µA in backscatter mode, and a working distance of 10 mm. A combination of multi-point analysis and X-ray elemental mapping was employed. Specific areas to be examined for elemental composition with multi-point measurements were carefully selected onto SEM backscattered electron (BSE) images manually, making sure that the target areas on each layer were representative of the entire layer. X-ray elemental mapping was used to visualise the distributions of the elements present in each layer. The acquisition times (live time) for analysing each selected area and for producing the elemental maps were 60 s and 600 s, respectively.

Further investigations were conducted to determine the composition of the plaster in the same cross-section. Morphological examinations (SEM) and elemental composition (EDS) analyses were carried out using a Hitachi TM3000 scanning electron microscope coupled with an Oxford Instruments energy dispersive spectrometer, in the following conditions: working distance 8–12 mm, probe current 200 pA, accelerating potential 15 kV. All the EDS data are presented as oxides, measured as weight%, and normalised to 100%.

Images were captured at consistent magnifications (×200, ×1000, ×1200, ×2500) for the purpose of comparison. The analysis of the average size of grains was obtained using the software ImageJ. Maps of the elemental distribution of the different materials were obtained to evaluate similarities and differences in the composition of the plaster.

Proteomic analysis

Proteomics was performed on four samples (P1-P4, Fig. 8) on ÆIN 297. Despite no proteinaceous material being detected from the gilding preparation with FTIR, a sample (P1) was chosen for proteomics analysis to investigate the binding medium used for the gilding.

FTIR gave a positive indication of protein for samples S8 (purple paint, P2) and S9 (yellow paint, P3), which were therefore selected for further analysis. Sample (P4) was taken from the pink headband.

The chosen samples were transferred to separate Eppendorf Protein Lo-Bind tubes along with negative control to verify the authenticity of the proteins extracted and monitor laboratory contaminants. The samples were incubated at 80 °C for 2 h in 100 µL of an extraction buffer containing 2 M Guanidine hydrochloride (GuHCl), 10 mM TCEP (tris(2-carboxyethyl) phosphine), 20 mM CAA (2-chloroacetamide), and 100 mM Tris–HCl (trisaminomethane). After 2 h, 10 µL of supernatant was taken off for protein concentration using both Bradford and BCA assay.

Extracted proteins in solution were then subjected to a double-step enzymatic digestion. First, proteins were digested for 1 h at 37 °C with 0.2 µg of rLysC (Promega). The extract was then diluted to a final concentration of 0.6 M GuHCl using a dilution solution containing 50 mM tris, and 10% acetonitrile (ACN) in water. The second digestion step occurred overnight under agitation at 37 °C with 0.4 µg of trypsin (Promega). Samples were then acidified to around pH 2 using 10% trifluoroacetic acid (TFA) to quench the digestion as well as provide counter ions. To avoid blockage and the transfer of solid materials the samples were centrifuged for 5 min at 10.000*g* before the peptides were desalted and loaded on Evotips according to manufacturer's instructions (EVOSEP Odense, Denmark).

Peptides were separated on an 8 cm by 100 µm (3-µm particle size) C18 endurance column, EV1064 (EVOSEP), and analysed using an Evosep One (EVOSEP) chromatograph connected to a Q-Exactive HF mass spectrometer (Thermo Scientific). The Evosep One method was set to the standard 60 SPD (21-min gradient, cycle time of 24 min, solvent A; 0.1% formic acid in water, solvent B; 0.1% formic acid in 100% acetonitrile). The Q-Exactive HF was operated in data-dependent top-12 mode for MS/MS. Mass spectra were recorded at a mass resolution of 120,000 at m/z 200 over the m/z range 350–1600 with a target value of 3e6 and a maximum injection time of 100 ms. HCD-MS/MS generated fragment ions were recorded with a maximum ion injection time set to 100 ms and a target value set to 1e5 and recorded at a mass resolution of 30,000. The normalised collision energy was set at 28% and the isolation window was 1.2 m/z with the dynamic exclusion set to 3 s and a charge state exclusion of 1, 5–8. A tryptic digest of bovine serum albumin was used for quality control of the LC–MS setup and a blank control was run prior to the samples to estimate the LC–MS background.

To determine the possible sources of protein in the sample, the palaeoproteomic data of the four samples from ÆIN 297 was analysed with novor.cloud (https://novor.cloud/), a free online proteomics mass spectrometry data analysis software. The following settings were used: built-in nr.fasta database, with Carbamidomethyl (C) as fixed PTMs, Pyro-Gly (Q), Carbamidomethyl (DHKE), Pyro-Glu (E), Sodium (DE), hydroxyproline, Oxidation (FHMW), Deamited (NQ) as the variable PTMs, with other default settings. The resulting peptide list was filtered to analyse just the peptides that were characteristic of 1 or at maximum 5 proteins in the mixture, to be able to differentiate more precisely from a family level to a specific species level.

Peptides were compared with protein groups to match identification codes and species names and then re-evaluated to obtain characteristic peptidic chains and assess spectrum coverage, with ions b + and y + utilised to estimate good matches, particularly in the deamidated sections. The best overlap between an animal species and the peptide was established with pBLAST [34]. Only peptides resulting in a coverage of 100% with an overlapping peptide chain of 100% were included in the downstream analysis. Furthermore, contaminants originating distinctly from laboratory processes, such as those found in the extraction blank, and from handling, such as keratins, were excluded from the final analysis. The plausibility of the results was also mirrored by the nature of the samples, the geographic origin of the sample, and the age of the sample.

Results and discussion
Textiles
The textiles were recorded in five areas (Fig. 3a):

1. The front of the mask, over the right wrist and along the bottom edge of the piece (hereafter named Main Front Break—MFB).
2. On the right side of the plastron, over the tunic edge on the exterior of the left arm (hereafter named Arm).
3. On the left side over the mantle's edge (this area was too badly preserved to be much instructive).
4. On the back of the head, over the falcon's tail and along the bottom edge (hereafter named Back of the head—BH).
5. And at the back, on the left side over the right temple.

The objectives of the textile analysis were to (i) determine the main technical traits of the textiles, and (ii) try to identify the different layers of fabrics across the entire object. The visible layers of the textiles indicate that the textiles were placed flat and not coarsely agglomerated. It is unclear if the same textiles were present over the entire artefact, or if smaller pieces of reused fabrics were superposed in different areas, in a sort of patchwork pattern. The main break at the front shows that the textile layers were most probably folded over themselves to form the edge of the mask, in effect hiding the superposition of textiles that might have been visible along the sides. The well-preserved painted surface and the current mount preclude any "cross-section" view of the complete structure of the mask.

In the main frontal break, visual observation clearly shows two different types of textiles. One coarser textile (Textile 1), of which two layers can be recognized along fresh breaks in the plaster, there and in other locations, and a finer textile underneath (Textile 2), which is only attested in this area. It is impossible to determine if "Textile 1" was represented by one fabric folded over into several layers or by two individual layers of similar but not identical fabrics. As such, these labels remain arbitrary, designating a type of fabric more than individual pieces.

Because of the difficulties in accessing the textiles with magnification tools, only four recording points could be found. As no edges were recorded in the present locations, it was not possible to distinguish weft (horizontal) from warp (vertical) threads, so the categories System 1 and System 2 were adopted instead. For all recorded points, one system was clearly dominant over the other and was consistently recorded as System 1. Based on the linen weaving tradition of Pharaonic and Greco-Roman times, which favoured warp-faced fabrics [35, 36], it is possible that this dominant system was the warp.

All textiles recorded show a plain tabby weave, in a simple 1/1 structure with one system (System 1) dominant over the other (Table 1).

The category Textile 2 exhibits many more threads in System 1 than in System 2, and for this reason can be tentatively qualified as "warp-faced". This feature is amplified by a clear difference in thread diameter between the two systems, with significantly thinner threads in System 1. The whole appearance of the fabric is consequently much finer and denser than Textile 1 (Table 2).

The category Textile 1 cannot be described in such a cohesive manner, as each location shows slightly different measurements. Degraded areas tend to be more open and distended, while better-preserved areas are showing a denser and more regular weave. Comparing both the thread diameter and thread counts indicate the technical proximity of the fabric located at the back of the head (BH) and the upper arm (Arm), while the one located in the Main Front Break (MFB) stands a little aside. This could potentially indicate that two different fabrics were used in these two locations, but the differences are not
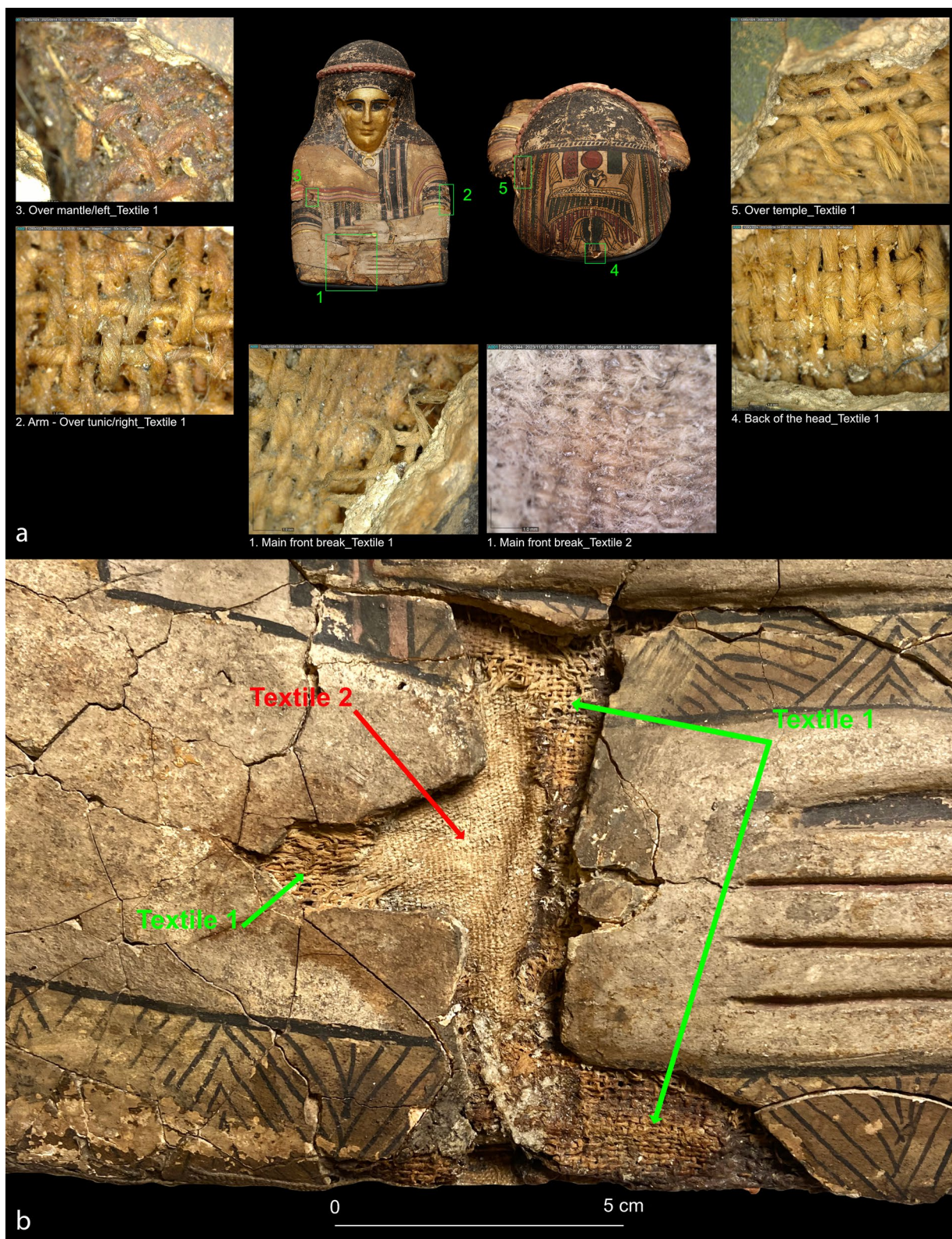
Kasso *et al. Heritage Science*   (2024) 12:250

Page 9 of 22

Fig. 3 **a** Areas 1–5 of ÆIN 297 recorded for textile analysis. DinoLite photographs, magnification between ×45 and ×50). **b** Detail of the mask's lower edge, with the area "main front break" showing the two different types of textile: Textile 1 (green arrows) and Textile 2 (red arrow)

Kasso *et al. Heritage Science*   (2024) 12:250

Page 10 of 22

Table 1 General technical features of the textiles

Location	Textile type	Max. size visible	Weave	Thread count/cm		Thread twist direction	Fibre
				S1	S2		
Main Front Break (MFB)	Textile 1	9×5 cm	Tabby, 1/1	10	6	S	Plant
	Textile 2	7×4 cm	Tabby, 1/1	26	10	S	Plant
Arm	Textile 1	2.5×1 cm	Tabby, 1/1	14	8	S	Plant
Back of the head (BH)	Textile 1	1×1 cm	Tabby, 1/1	16	8	S	Plant

Table 2 Thread diameter per system, for each textile, showing a rather high range of possibilities (10 measurements were recorded for each system)

Diameter in mm	MFB/textile 1		MFB/textile 2		BH/textile 1		Arm/textile 1	
	S1	S2	S1	S2	S1	S2	S1	S2
Minimum	0.55	0.50	0.26	0.51	0.41	0.52	0.48	0.45
Average	0.64	0.63	0.40	0.61	0.55	0.66	0.57	0.59
Maximum	0.81	0.75	0.51	0.80	0.63	0.79	0.74	0.64

sharp enough to be categorical. They simply may be due to preservation.

The threads exhibit a rather wide range of diameters, from 0.26 mm to 0.81 mm, the same thread frequently exhibiting sharp differences along its length. They are all twisted in the S direction (counter-clockwise). The area BH was well preserved enough to allow the recording of the spin angle (10 measurements in System 1 and 6 in System 2). The spin angle ranges from 21° to 49°, with a higher spin used in System 2—with an average of 43° in System 2 and 32° in System 1. However, the small amount of measurements available does not offer many conclusions.

On the small areas documented, no plied thread was recognized: all threads seem to have been made of one single element, regrouping the fibre bundles in a clear S torsion. The absence of plying and the overall aspect of the threads differentiate them from the Pharaonic production of spliced threads [37, 38], but the very limited size of our sample does not allow us to securely identify them as spun threads either. Considering the time period, however, it is a reasonable assumption.

All observations have indicated the textiles to be made of plant fibres. The samples from Textile 1 show a lot of impurities and extraneous material, probably dust and conservation material accumulated through the years of being exposed. Fibres from Textile 2, comparatively more protected since being the lower layer, appear much clearer. In both cases, the longitudinal views of the fibres show straight fibres with a typical polygonal shape and a thin lumen, with thick crossing nodes (Fig. 4a and b). These nodes appear as horizontal lines crossing the fibre perpendicularly and often present weak points where the fibres tend to break. This is characteristic of bast fibres, typically of flax [39]. The use of flax has been characteristic of Egyptian textiles since the very beginning of their production and continues to be a staple for funerary wrappings of all nature until late in the Roman period [35, 40].

Despite the limitations imposed by the preservation of the mask, it was still possible to document the basic manufacturing traits of the fabrics and to give hints as to the superposition of different textiles to form a solid yet partly flexible artefact, able to be moulded into an anthropomorphic figure. In the areas available for study, it is noteworthy to point out small particles of a reddish material (possibly a resin) that seem to have been placed sporadically in between the textile layers (see Fig. 3a). Plaster particles are also adhering to the uppermost layers of the textiles, embedded in the threads, showing that partially wet plaster probably seeped through a little and reminding us at microscopic level of the composite nature of such mummy masks.

Overall, the different fabrics recognized in ÆIN 297 seem to fit well in the textile production landscape of the time period in the oasis [41]. The use and reuse of textiles for body wrappings, cartonnage, and plaster masks remained a hallmark of the Greco-Roman funerary arts when immense quantities of textiles were assembled to develop the mummification industry for both humans and animals [35, 40].
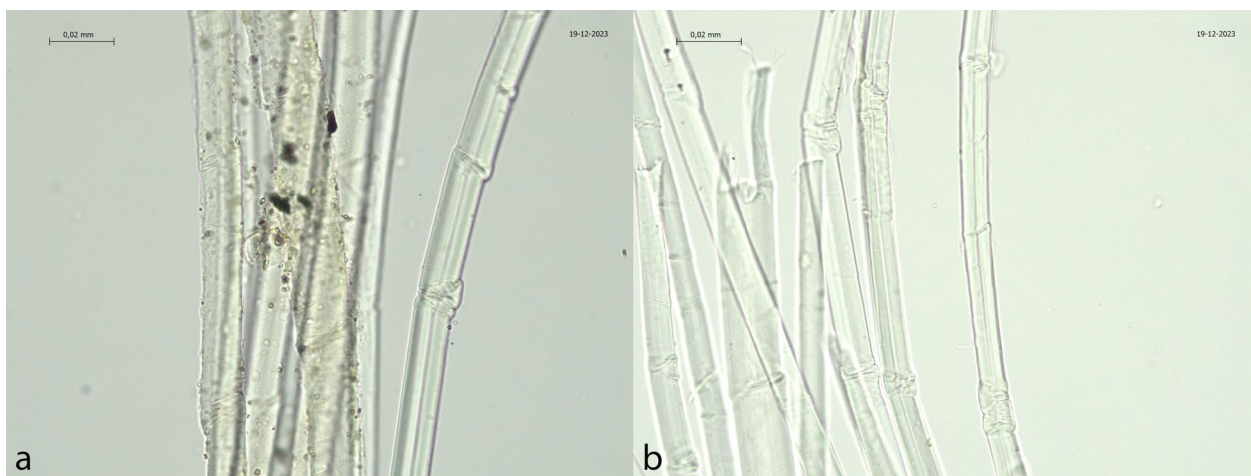
Fig. 4 a Flax fibres from Textile 1. **b** Flax fibres from Textile 2. Both photographs were taken at ×63 magnification, on a Leica DM750 transmitted light microscope

Plant fibres

Plant fibres with a dark adhesive were used to render the hair, probably arranged in a way to imitate an elaborate black hairdo or a wig. Fashionable among the elite during the Roman period, wigs or smaller hair pieces were often made from palm fibre or grass [42, 43]. Additionally, similar species, let alone different fibres could have been used together for the hair [44]. The material in ÆIN 297 is thick, and grass-like, and only fragments of it remain on the surface of the mask.

Based on visual inspection of the fibres from the hair-area of ÆIN 297, and taking into account the tradition of wig-making, it is likely that the material used for the hair is a kind of grass or reed (Fig. 5a–d). Stylistic comparison of ÆIN 297 to similar contemporary masks with preserved hair (e.g. Ägyptisches Museum und Papyrus-sammlung, Staatliche Museen zu Berlin, inv. nos. ÄM 34435 and ÄM 34436) would suggest a curly hairstyle (Fig. 5a and b). The initial processing from raw material to finished product alters the appearance of fibre and can completely remove identifiable features [44]. In addition, degradation and changes to the fibres due to the post-depositional conditions may cause challenges to the correct morphological identification of the fibres [44, 45]. Here, the sheer fragility of the fibres made it very difficult to identify the plant species further.

Plaster

Plasters are artificial stone materials, usually characterised by a mixture of aggregates and binders, employed as coatings on masonry as the most external and final layer or on surfaces as preparatory grounds, to prepare them for painting and gilding [46]. Applied as single or multiple layers, plasters were obtained by the chemical change through the heat of natural rocks, which were then crushed to a very fine powder and mixed with water, to obtain an easily spreadable plaster with better mechanical and physical properties once dried [47]. Commonly made from mud, gypsum and lime, plasters were widely employed in Egypt for architectural and artistic purposes, as described by Lucas [48, 49].

However, it is important to acknowledge that, in Egyptology, the term plaster has been used rather loosely, without a specific chemical definition and it includes different kinds of materials and preparations [50]. Depending on the type of treatment the raw material underwent (crushing, heating at different temperatures), the final plaster will look different from a microscopic level, especially under the electron microscope. In this way, it should be possible to differentiate between the presence of clay, gypsum (treated and untreated) and limestone (treated and untreated). In the case of heated gypsum, the characteristic needle structure of the grains should be visible under the microscope, very different from the morphological appearance of the natural and untreated gypsum.

Regarding the presence of calcite, previous studies [51–53] have shown the possibility of using the size of calcite grains to differentiate real plaster (treated with heat until a complete recalcination of the original material) from plasters made of crushed limestone. Real plaster should have a grain size < 1 μm, due to the complete re-calcination of the material [51, 52].

When preparing the sample as a cross-section, it split into two pieces: since the analytical measurements from both parts were consistent, the results from only one of them are included in this publication. When observing the morphological appearance of the plaster material

Kasso *et al. Heritage Science*   *(2024) 12:250*

Page 12 of 22

Fig. 5 a, b Details of "hair" on ÆIN 297 (on the left) and ÄM 34435 (on the right). **c, d** Fragment of the plant fibre used to render hair on ÆIN 297. Both photographs were taken at ×10 magnification

under SEM, the absence of calcite particles and the characteristic needle-shaped structure of gypsum is clear (Fig. 7) [54]. This morphological appearance supports the idea that the gypsum had been treated with heat before its application on the mummy mask, making it a gypsum plaster. The presence of gypsum as bulk material for the plaster can also be confirmed through the EDS analysis (Fig. 6), in which sulfur (S) and calcium (Ca) are the two major elements in the mixture. Silicone (Si) in the form

of silicates is a minor component just scattered on the surface [54], which could suggest that it derives from ceramic containers or is an impurity in the raw materials used (Fig. 6).

FTIR (see Supplementary Material 2 for spectra) was employed to confirm the previous results obtained with SEM–EDS. Our measurements confirmed the previous hypothesis of gypsum as the main component of the plaster. The absence of impurities and the presence of a peak

Kasso *et al. Heritage Science*   (2024) 12:250

Page 13 of 22
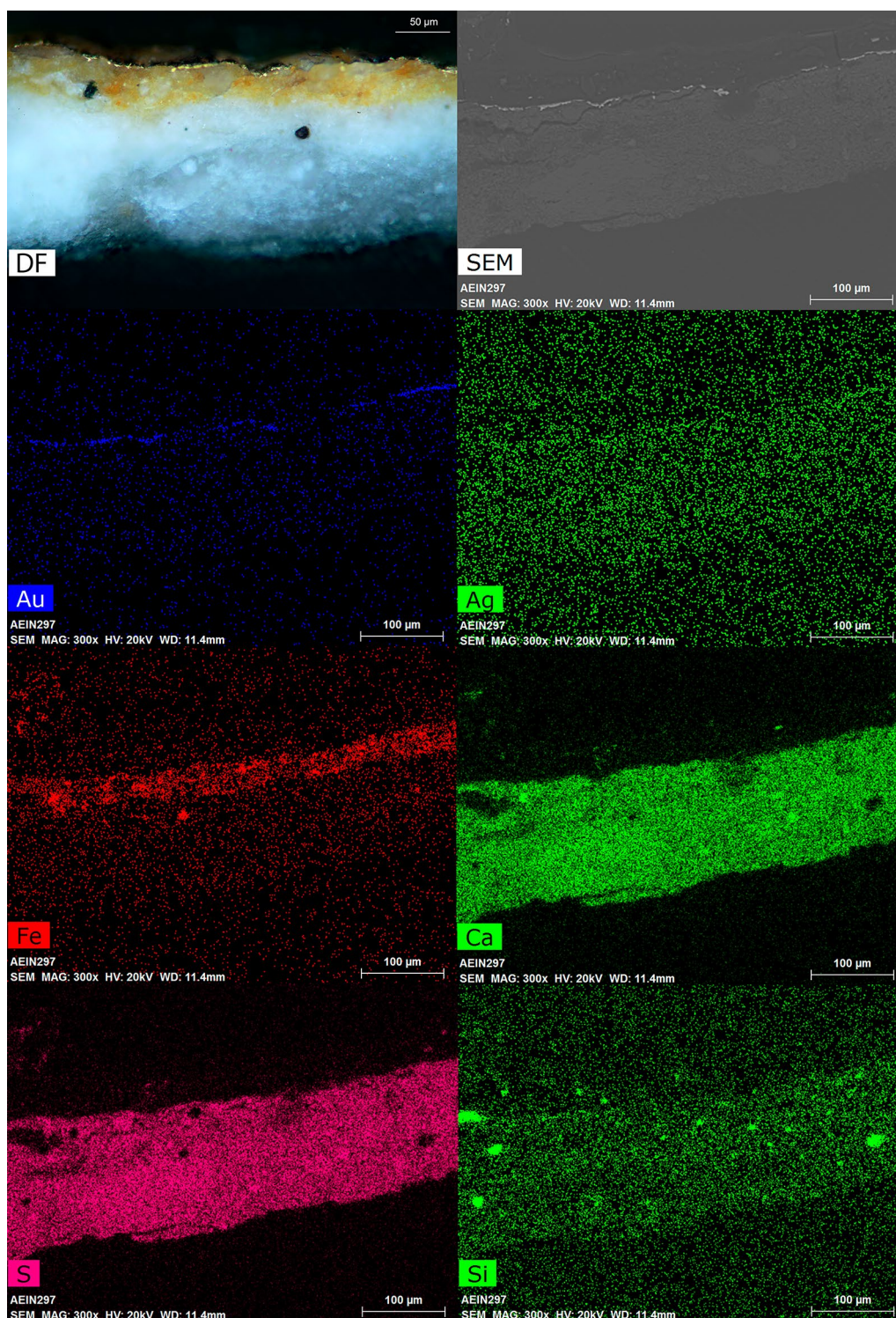
Fig. 6 Darkfield (DF) visible light image, SEM backscattered electron image, and SEM–EDS elemental maps of the cross-section of the gilding and its preparatory layers from the face of the mummy mask. The gold leaf is primarily gold (Au) with small amounts of silver (Ag). The concentration of iron (Fe) in the yellow layer of the gilding preparation could indicate the use of yellow ochre. Key elements for the plaster are calcium (Ca) and sulfur (S), with some inclusions of silicate (Si)
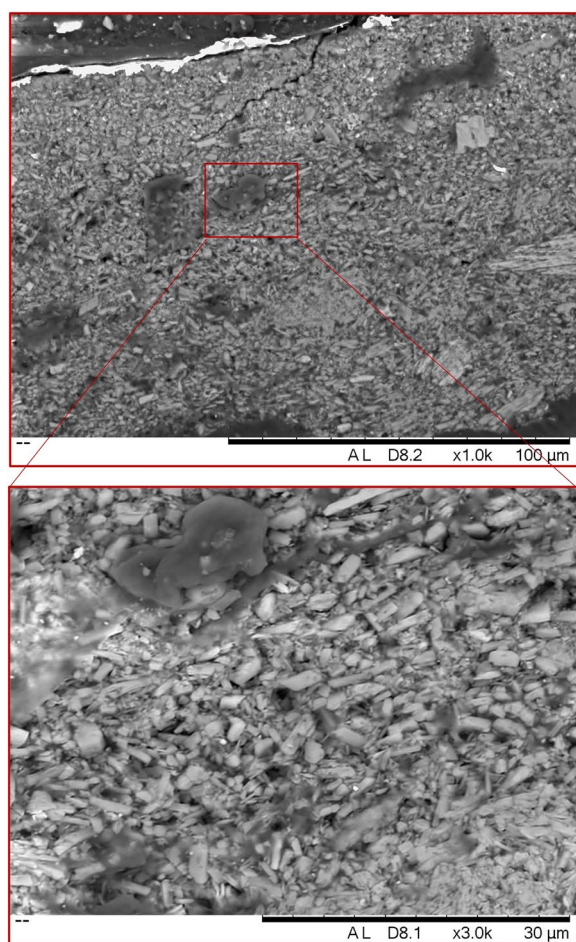
Fig. 7 SEM images of the cross section of ÆIN 297 with the characteristic needle-shaped structure of gypsum

at 1107 cm^{-1}, typical of the anhydrite structure, support the idea that this material had been treated with heat before application [55–58]. Calcite was present in the plaster in a very small amount and it hasn't been detected in all the samples.

In the samples in which a signal was present, the $\nu2/\nu4$ ratio was calculated. The ratio between the $\nu2$ peak (815 cm^{-1}) and $\nu4$ peak (712 cm^{-1}) represents the extent of the atomic disorder in the calcite structure due to heating and can give an idea of the pyrotechnology employed for the preparation of this plaster [59]. If the result is between 3.3 and 7.7, this means it has been treated with heat and, therefore, it is a real plaster [59].

Based on the measurements on ÆIN 297, the calcite present in the samples would have been treated with heat at a very high temperature, guaranteeing complete calcination of the original limestone. This is consistent with the plastering technology in the Roman empire and its provinces for both architectural structures and artworks [57, 60]. Moreover, as material only from the area of the

face of ÆIN 297 is analysed, the possibility that plaster of different combinations was used elsewhere in the mask cannot be excluded.

Gilding

Gilding used for the face was customary in Egyptian funerary art of the elite [5, 6]. Despite the production of gold leaf has usually been thought to be made with highly refined, pure gold, investigations of Egyptian gold leaf show a wide variety in composition [61]. In the ancient world, gold was processed for use through cupellation and parting. Cupellation removes the minor impurities (copper, lead) but amounts of silver usually remain, and this could then further be removed with parting [61]. Parting requires strong acids that became more available in the medieval period, thus the majority of ancient golden or gilded artefacts have amounts of silver [61].

The composition analysis is further challenged by the surface evaporation of most reactive metals from the alloy. This may happen as a consequence of an original ancient surface treatment, due to the burial environment, or from a modern chemical conservation treatment [16, 61]. Additionally, a segregation of the alloy may occur, which leads to the enrichment of one metal on the surface. This is known to happen in gold-silver alloys, leading to a continuous enrichment of silver on the surface [16]. Therefore, estimations of the apparent purity or quality of the gold can only be tentative [16, 62].

The analysis with SEM–EDS of the gold leaf with elemental mapping can be seen in Fig. 6. See Supplementary Material 1 for SEM–EDS spectra obtained from the top surface of the sample. The gold leaf primarily consists of gold (Au) with small amounts of silver (Ag). The concentration of iron (Fe) in the yellow layer of the gilding preparation would indicate the use of yellow ochre, but it is also found as a trace element in Egyptian gold [62]. Unadulterated gold usually contains some amount of silver (5–30%, up to 50%), some copper (> 1–2%) and other impurities [61, 62]. Small amounts of silicon (Si) in the gold may be the remains of the original mineralized quartz veins, from which the gold was sourced in ancient Egypt and Nubia [61, 62] (Fig. 8).

Constituents of paint
Pigments
As seen from Table 3, a wide range of pigments and adhesives were used in the construction of ÆIN 297.

VIL imaging of the back of the mask showed some condensations of vividly luminescing particles in the green areas (Fig. 9), indicating the use of Egyptian blue. The detected quartz and kaolinite in the FTIR analysis indicates that the Egyptian blue was mixed with yellow ochre to create the green hue used to render a part of the motif.
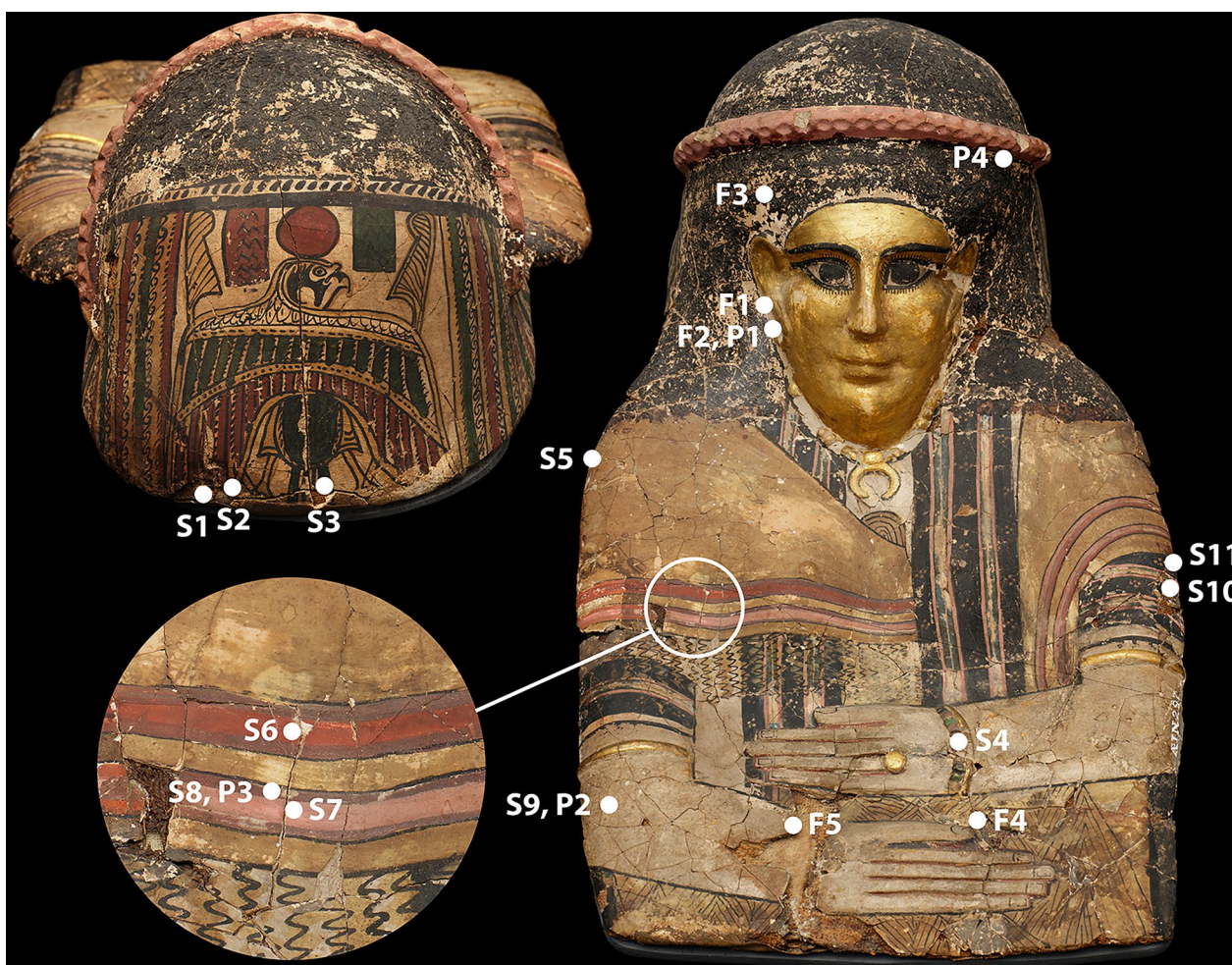
Fig. 8 Sampling areas of ÆIN 297 for analysis

VIL imaging (Fig. 10) reveals a strong luminescence in the blue stripes for the *clavi*, which suggests the presence of Egyptian blue ($CaCuSi_4O_{10}$) [63]. The presence of Egyptian blue in the *clavi* was confirmed by FTIR analysis (peaks 1260 cm^{-1}, 1160 cm^{-1}, 1064 cm^{-1}, 1008 cm^{-1}, 756 cm^{-1}, 668 cm^{-1}).

The purple colour used for the bands of the mantle and some of the beads in the bracelet was created by a mixture of indigo and red ochre (Fig. 10).

In a sample removed from the green bracelet copper stearate and copper oxalate were identified by FTIR spectroscopy (Fig. 11, Table 3). Possibly, small amounts of other copper soaps are also present. Metal soaps and metal oxalates often occur as degradation products of aged paint. The degradation of copper-containing pigments such as atacamite and malachite has been described by Scott [64, 65]. In his review from 2016 [64] he discusses the origin of copper organometallics such as copper-proteinate, copper carbohydrate, and copper wax

pigments in the context of pigment binder interaction. Copper soaps and copper oxalate are not mentioned.

Metal soaps have been discussed widely as a degradation phenomenon in oil paint where the metal cation from a pigment forms a salt with a free fatty acid stemming from the drying oil [66]. However, it remains unclear if the copper soap identified here is a degradation product or a deliberate production. It could be speculated if the original painting material was a copper-green oil paint but in this case all of the original oil would be converted to soaps and degraded by microbial activity to oxalates.

Oxalates have been observed as degradation products on cultural heritage objects often as calcium oxalate since the mid-nineteenth century [67]. Recent findings include ancient Greek marble fragments [68] and ancient panel paintings from the Roman period in Egypt [9]. Copper oxalate has been found in bronze corrosion [69] on an exterior wall painting [70], and as the naturally occurring

Table 3 Overview of the results

Sample ID	Description	Pigment	Medium	Analytical method
F1	Plaster	–	–	FTIR
F2, P1	Gilding Gilding preparation	Silver-containing gold leaf Yellow ochre (iron-rich)	Gypsum plaster Collagen-based animal glue (*Equus asinus*)	FTIR, SEM–EDS, proteomics
F3	Hair adhesive	–	Carbohydrate (gum)	FTIR
F4	Shiny glue (modern conservation treatment)	–	Protein	FTIR
F5	Matte glue (modern conservation treatment)	–	Nitrocellulose	FTIR
S1	Head, red	Red ochre (gypsum, quartz)	–	FTIR, UVF
S2	Head, yellow	Yellow ochre (gypsum)	–	FTIR, UVF
S3	Head, green	Yellow ochre (quartz, kaolinite) Egyptian blue	–	FTIR, UVF FTIR, VIL
S4	Bracelet, green	Copper-based green (copper stearate, copper oxalate)	–	FTIR
S5	Mantle, yellow	Yellow ochre (talc, alum)	–	FTIR, UVF
S6	Band, red	Red ochre (quartz)	Carbohydrate (gum)	FTIR, UVF
S7	Band, pink	Organic red lake (fluorescence)	–	UVF
S8, P3	Band, purple	Red ochre (kaolinite) Indigo	Collagen-based animal glue (*Equus asinus,* *Gallus Gallus*)	FTIR, UVF MBR Proteomics
S9, P2	Skin, yellow	Yellow ochre (gypsum, goethite)	Collagen-based animal glue	FTIR, UVF, Proteomics
S10	Band, Blue	Egyptian blue	–	FTIR, VIL
S11	Band, Black	Carbon black (quartz, gypsum)	–	FTIR, UVR, IRR
P4	Headband, glue	–	Collagen-based animal glue	Proteomics

See Supplementary Material 2 for FTIR spectra
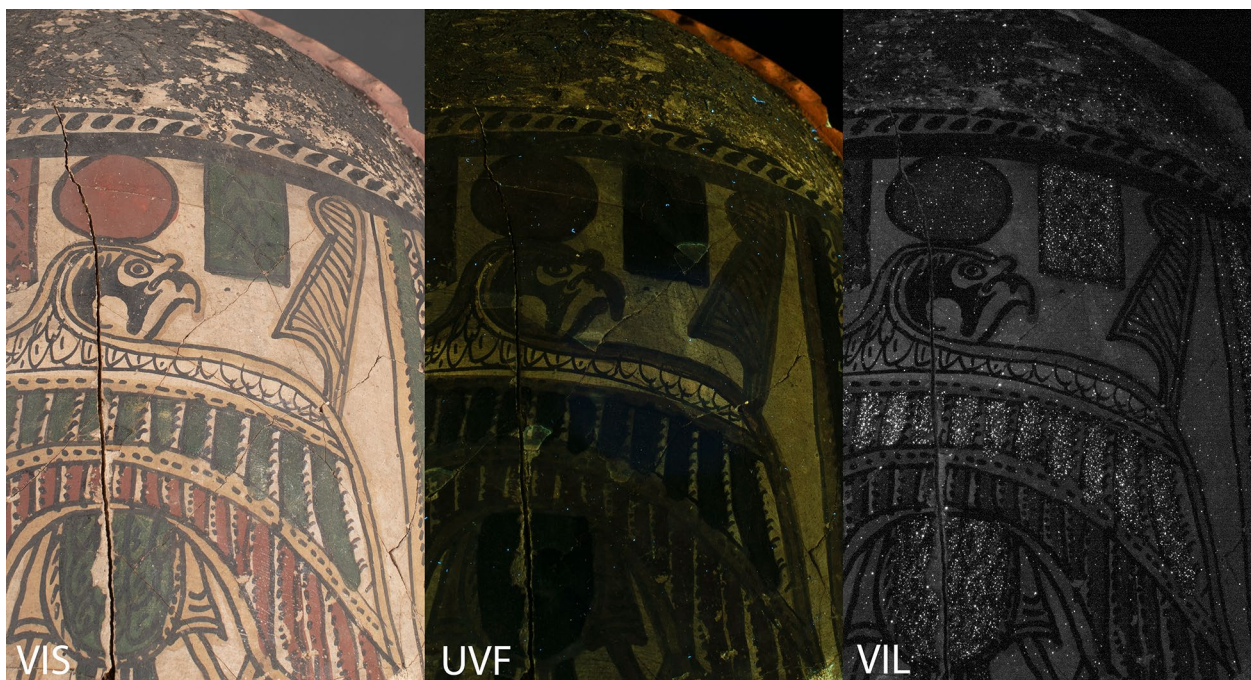
Fig. 9 Detail of the back of ÆIN 297. Visible light photograph (VIS) (left). In the UVF image (centre) the painted red and yellow areas are dark, which suggests the presence of earth pigments (ochres). Note the bright fluorescence of an organic red lake on the headband. The VIL (right) image shows the bright luminescing particles of Egyptian blue in the areas with green paint
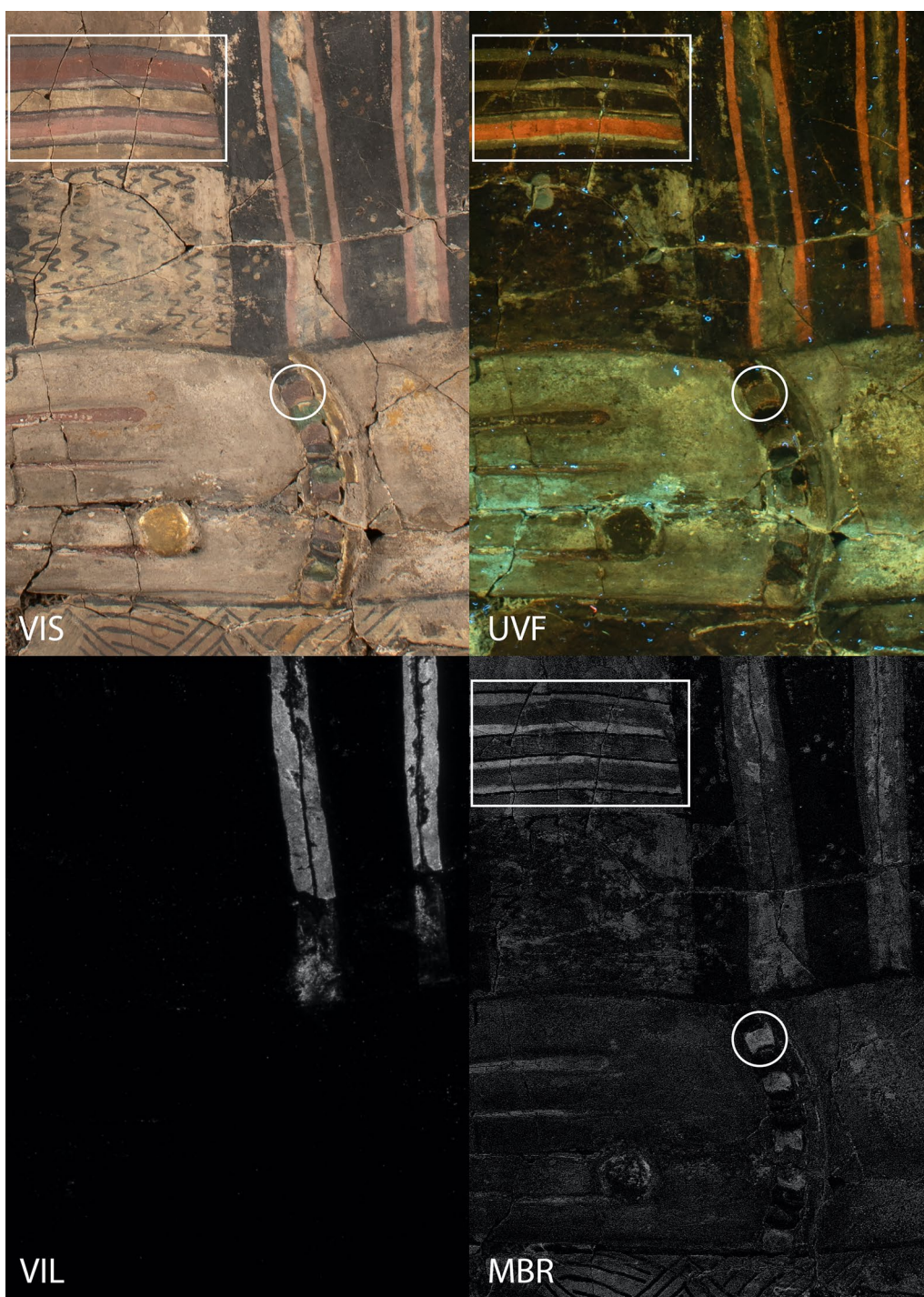
Fig. 10 Detail of ÆIN 297. The purple bands on the tunic and the purple beads of the bracelet (VIS) fluoresce in light to medium blue-grey under UV light (UVF). Additionally, UVF reveals a strong light blue fluorescence produced by the nitrocellulose glue used for the conservation treatment. No luminescing particles indicative of Egyptian blue are observed in the purple paint (VIL). The same areas appear light grey in the MBR image, suggesting the presence of indigo

mineral which has the name moolooite (https://cameo.mfa.org/wiki/Copper_oxalate). Zoppi et al. discusses the reactivity of different copper-based pigments in the

presence of oxalic acid. The occurrence in the present study seems likely another degradation case [71].

Kasso *et al. Heritage Science*   (2024) 12:250

Page 18 of 22
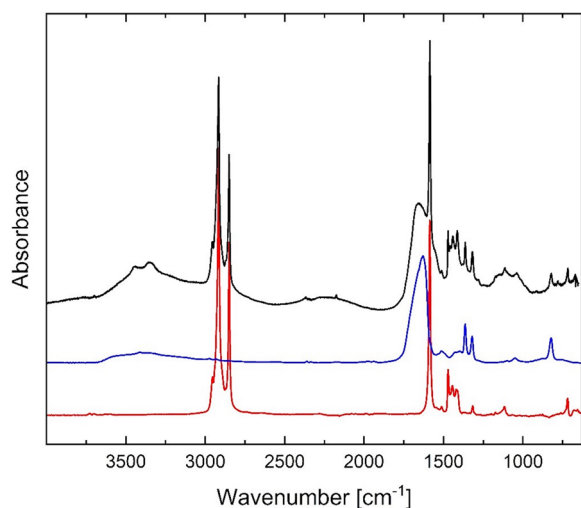
Fig. 11 FTIR spectrum of the sample (black) of the green paint used for the bracelet of ÆIN 297. References shown are copper stearate (red) and copper oxalate (blue). Copper oxalate reference spectrum courtesy of Dr. Stefan Zumbühl, (Hochschule der Künste Bern)

For the red paint, red ochre was used on the back of the head as well as in combination with indigo to create purple to render the garments. Moreover, an organic red lake was used for the pink stripes or bands of the tunic and the pink headband, as attested by its

characteristic bright orange fluorescence under UV light (Figs. 10 and 12).

Yellow ochre was used throughout the mummy mask, including in the preparatory layer for the gilding, on the skin of the arms and in the painted garments (Fig. 12), and on the back of the mask. The identification of the yellow pigments with FTIR was difficult due to the presence of plaster in the sample, which obscured the results. However, the SEM–EDS analysis (Fig. 6) shows a concentration of iron (Fe) in the yellow layer of the gilding preparation, which suggests the presence of yellow ochre. The yellow areas of the skin and garments are visibly dark under UV light, which supports the presence of yellow ochre [72].

The identification of white pigments from a plaster surface is challenging, as some white pigments such as gypsum and kaolinite can also be present in the plaster, and can therefore transfer to the paint. However, it is equally plausible that some previously mentioned white inorganic pigments were used in the paint: for example, the presence of kaolinite in the purple paint (Table 3) could indicate this. Finally, black paint was rendered with a carbon-based black throughout ÆIN 297, as seen from the very dark areas in the UVR images (Fig. 12).

As shown in Table 3 above, numerous pigments and colourants were used for the polychromy of ÆIN 297. Most of them are commonly used in ancient Egyptian polychromy in the Roman period and hence to
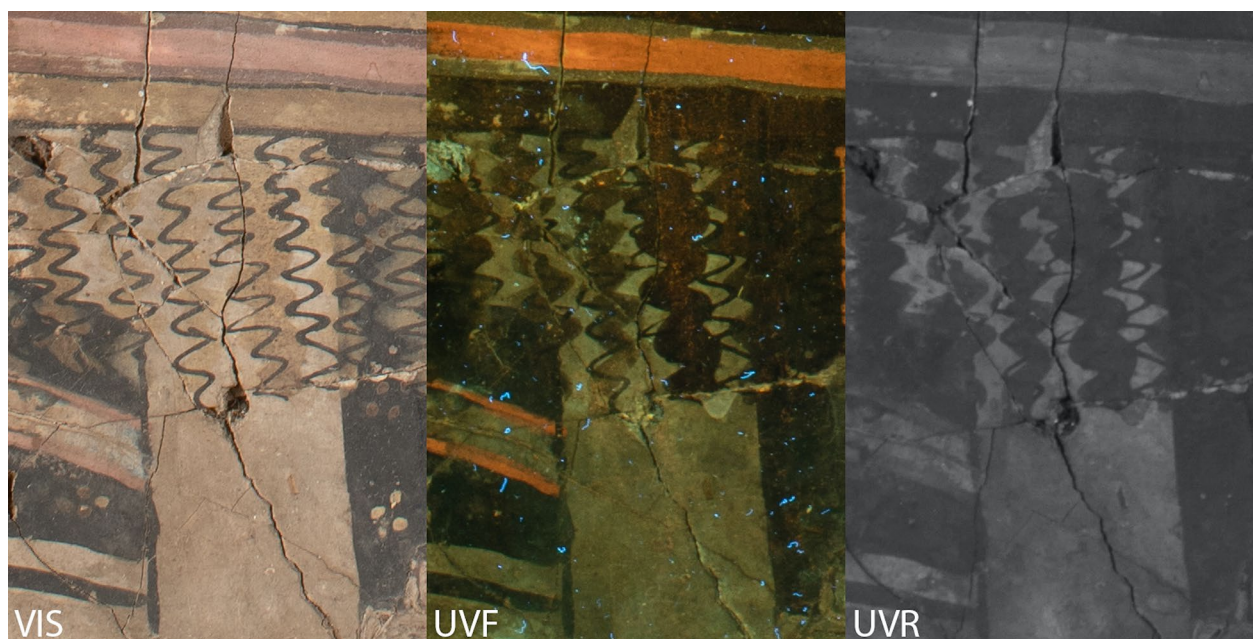

Fig. 12 Detail of ÆIN 297 showing the edge of the mantle painted with yellow ochre and the two layers of the fringe of the mantle. A thicker set of fringes was first painted with a light yellow paint, and another set of fringes (or the outline of the first set) was then painted over with carbon black

be expected for an artefact such as this [9, 10, 73]. This includes naturally occurring earth pigments such as yellow and red ochre, which have been in use since prehistory as a pigment for painting [74]. Similarly, carbon-based black, used for painting various parts of ÆIN 297, is a very common black colourant, and in comparison, the most commonly attested black pigment in contemporary Romano-Egyptian panel paintings [9].

The blue paint used for the *clavi* is rendered with the bright, crystalline pigment Egyptian blue. Egyptian blue is almost omnipresent in ancient polychromy from the 3rd millennium BCE onwards [75, 76]. In Romano-Egyptian panel paintings, for example, it is commonly used to render blue as well as in mixtures. The organic blue colourant indigo is also attested on ÆIN 297. However, it is not used alone, but in a mixture with red ochre to render purple. This use of indigo appears to be typical of Romano-Egyptian polychromy, where it tends to be used in mixtures with other pigments, but never alone to render blue for which Egyptian blue was used. Moreover, it is interesting to note that Egyptian blue and indigo do not appear to be mixed, and only very rarely are the two attested for the polychromy of the same artefact. One such rare example is a Romano-Egyptian votive panel, depicting the goddess Nemesis and Harpocrates (NCG, no. ÆIN 685). In this panel, both indigo and Egyptian blue are used, but they are used for different parts of the polychromy [9]. Perhaps this exclusive use of the two blue pigments could suggest that they were considered distinct colours or hues. However, it should be kept in mind that there might be a bias in the methods of analysis, as Egyptian blue is much easier to identify due to VIL photography, while indigo is more challenging to attest in ancient polychromy.

The analysis of ÆIN 297 also revealed the use of an organic red lake to render the pink hue of the pink flower garland and pink on the *clavi.* The strong fluorescence in UV light is usually assumed to suggest the use of madder lake. However, other organic red lakes were available in antiquity, such as lac and kermes [77].

Finally, the polychromy of ÆIN 297 includes various pigment mixtures used to obtain different hues. This includes, for example, mixing Egyptian blue with yellow ochre to obtain a green colour as well as the mixture of indigo and red ochre to render purple, as already mentioned above. Such paint mixtures were a normal feature of Egyptian polychromy in the Roman period, and are commonly attested in for example panel paintings [9, 78].

Binding media and adhesives

Two types of adhesives were identified as constituents of the polychromy: gum, and a collagen-based animal glue. The type of medium influences the overall appearance of paint, contributing to variations in texture, glossiness, and colour saturation. Gum was identified with FTIR from two samples (F3, S6) used both as an adhesive to arrange the plant fibre hair on ÆIN 297 and as a painting medium in the red bands of the mantle. Based on the darkened appearance of the blue bands painted with Egyptian blue, gum was specifically used as a medium in these areas [79]. For example, gypsum turns grey when used with gum [72], which could partially explain some of the dullness of the colours in ÆIN 297.

Sample S6 matched locust bean gum with FTIR, but this cannot be taken as a verification for species identification. It has been suggested that locust bean gum was used in mummification processes [80, 81], although Newman and Serpico (2000) argue against the extensive use of locust bean gum due to its difficult preparation [82]. However, more recent investigations support the use of gum as an adhesive in Egypt during the Roman period [83]. Species from two genera produce the gums which were probably most widely available in ancient Egypt: *Acacia* spp and *Astragalus* spp [82]. Gum was not identified elsewhere, but was likely used both as a paint medium and as the adhesive for hair fibres in ÆIN 297.

The proteomic analysis identified the likely species ID's for protein sources for samples P1 (gilding preparation) and P3 (paint medium). Sample P1 is a collagen-based animal glue with a dominant peptide that matches *Equus asinus* (donkey). Sample P3 also had frequent peptide matches to *Equus asinus*, but also some to *Gallus Gallus* (chicken). Notably, the purple band from which the sample P3 was taken, lays on top of a pink paint layer, hence P3 may be a measurement of two separate layers together. This could indicate that the painting medium was a mixture of animal glue and tempera, but an apparent mixed medium could also be explained by a dirty brush, or due to the overlapping of layers.

Donkeys were a main way of transporting and they could also reach remote sites in Egypt [84], such as oases. Therefore, making use of donkey remains as glue and as a binding medium is not surprising. The presence of animal glue in the gilding preparation, suggests the use of a gesso-like layer to which the gold leaf was applied on [62].

Other identified species with palaeoproteomics in very low amounts were *Sus scrofa* (wild boar) in P1, several species of Mus (mice) in P2 and P4, *Hyena Hyena* (hyena), P1–P3, *Hippopotamus amphibius* (hippo) in P2, *Bos taurus* (cattle) in P2–P4. Wild animals (wild boar, hyena, mice) could have been hunted and kept in captivity for meat and other products [85] alongside regular husbandry of animals such as cattle. Hippos were hunted for 'pest control' due to their harm to crops, and for their ivory [86]. Whereas it could be possible for a "waste-bin"

Kasso *et al. Heritage Science* (2024) 12:250

Page 20 of 22

source for the animal glue used combining waste of multiple animals, some of these species may be present as contaminants, or due to the poor annotation of some protein sequences in databases, so their intentional presence cannot be verified.

Conclusions

Currently, this investigation of ÆIN 297 is the first comprehensive analytical study of an object of this type. Therefore, the results are inaugural, yet can be linked to other contemporary artefacts from the same region and time period. The mask was made with plaster and likely repurposed linen, hence employing similar components following from centuries of mummy masks and their manufacture.

When comparing the mummy mask examined in this study to e.g. mummy portraits from the Fayum, it becomes evident that there are several similarities in the selection of pigments in funerary art during the Roman period in Egypt [9, 73]. It is likely that these pigments were easily accessible and in some cases even sourced or produced locally.

Two types of adhesives, gum and collagen-based animal glue, were identified in the polychromy, with gum serving as both adhesive and painting medium, impacting partially the current appearance of colours created with Egyptian blue. Proteomic analysis revealed *Equus asinus* (donkey) as a predominant protein source for the collagen-based animal glue, while additional species detected in low amounts may indicate potential contaminants or multiple sources for making the glue.

Comparative studies with similar artefacts from different regions within Egypt could offer insights into broader artistic trends and exchange networks. For example, as the identification of indigo is more challenging to attest in ancient polychromy, more knowledge of its use is needed. A wider investigation and analysis of additional mummy masks and other forms of funerary art from the Roman period in Egypt would also aid the characterisation of organic reds and the possible use of murex purple and improve the identification of such pigments.

Supplementary Information

Declarations

Ethics approval and consent to participate
Not applicable.

Competing interests
All authors declare no competing interests.

References
1. Root MC. Faces of immortality: Egyptian mummy masks, painted portraits, and Canopic Jars in the Kelsey Museum of Archaeology. Ann Arbor: Kelsey Museum of Archaeology, University of Michigan; 1979.
2. Peck WH. Mummy portraits from Roman Egypt: an exhibition organised by William H. Peck. The Detroit Institute of Arts, March 22-April 30; 1967.
3. Vandenbeusch M, O'Flynn D, Moreno B. Layer by layer: the manufacture of Graeco-Roman funerary masks. J Egypt Archaeol. 2021;107(1–2):281–98. https://doi.org/10.1177/03075133211050657.
4. Ikram S, Dodson A. The mummy in ancient Egypt: equipping the dead for eternity. London: Thames and Hudson; 1998.
5. Riggs C. The beautiful burial in Roman Egypt: art identity and funerary religion. Oxford: Oxford Studies in Ancient Culture and Representation Oxbow Books; 2005.
6. Andrews C. Egyptian mummies. 2nd ed. London: British Museum Press; 1998.

Kasso *et al. Heritage Science*   (2024) 12:250

Page 21 of 22

7. Rozenberg S. Earlier plaster masks from Sinai: forerunners to the Roman plaster masks. In: Bierbier ML, editor. Portraits and masks: burial customs in Roman Egypt. London: Trustees of the British Museum Press; 1997. p. 112–20.

8. Riggs C. Tradition and Innovation in the Burial Practices in Roman Egypt. In: Lembke K, Minas-Nerpel M, Pfeiffer S (eds) 2010. Tradition and Transformation: Egypt under Roman Rule. Culture and History of the Ancient Near East, 41. Leiden Boston: Brill; 2010. p. 343–356.

9. Brøns C, Stenger J, Newman R, Cartwright C, Di Gianvincenzo F, Katerinopoulou A, Ørsted Brandt L, Haghipour N, Hendriks L. 'A Lost Chapter of Ancient Art': archaeometric examinations of panel paintings from Roman Egypt. Stud Conserv. 2023. https://doi.org/10.1080/00393630.2023.2256132.

10. Cartwright C, Svoboda M (eds). Mummy Portraits of Roman Egypt Emerging Research from the APPEAR Project. Edited by Caroline Cartwright and Marie Svoboda, First edition. Getty Publications; 2020.

11. Borromeo GE, Neuman IA, Collins S, Cooper C, Marck D, Murray D. Framing the Heron panel: iconographic and technical Comparanda. In Svodoba M, Cartwright C (eds). Mummy Portraits of Roman Egypt. Emerging Research from the APPEAR. Los Angeles: J. Paul Getty Museum; 2020. p. 90–100.

12. Zesch S, Gander M, Loth M, Panzer S, Sutherland ML, Allam AH, et al. Decorated bodies for eternal life: a multidisciplinary study of late Roman Period stucco-shrouded portrait mummies from Saqqara (Egypt). PLoS ONE. 2020;15(11): e0240900. https://doi.org/10.1371/journal.pone.0240900.

13. Bradley L, Ford J, Kriss D, Schussler V, Pozzi F, Basso E, Bruno L. Evaluating multiband reflectance image subtraction for the characterization of Indigo in Romano-Egyptian funerary portraits. In: Svoboda M, Cartwright C, editors. Mummy portraits of Roman Egypt emerging research from the APPEAR. Los Angeles: J. Paul Getty Museum; 2020. p. 68–78.

14. Saleem SN, Seddik SAE, El-Halwagy M. Scanning and three-dimensional-printing using computed tomography of the "Golden Boy" mummy. Front Med (Lausanne). 2023;24(9):1028377. https://doi.org/10.3389/fmed.2022.1028377.

15. Schiavon N, Panganiban P, Valadas S, Bottaini C, Barrocas Dias C, Manhita A, Candeias A. A multi-analytical study of Egyptian funerary artifacts from three Portuguese museum collections. Heritage. 2021;4(4):2973–95. https://doi.org/10.3390/heritage4040166.

16. Gard FS, Daizo MB, Santos DM, Halac EB, Freire E, Reinoso M, Bozzano PB, Dominguez SA, Montero RJ. Application of surface science techniques to study a gilded Egyptian funerary mask: a multi-analytical approach. Surf Interface Anal. 2019;51(10):1001–17. https://doi.org/10.1002/sia.6685.

17. Ali MF, Mansour MMA, Badr NM, Salem MZM. A study of biodeterioration and chromatic alterations of painted and gilded mummy cartonnage at the Saqqara Museum Storeroom. Egypt Archaeometry. 2018;60:845–58. https://doi.org/10.1111/arcm.12340.

18. Corcoran LH. Portrait mummies from Roman Egypt (I-IV centuries A.D.): with a catalogue of portrait mummies in Egyptian museums. Chicago: Oriental Institute of the University of Chicago; 1995.

19. Rindi Nuzzolo C. The Excavations at Ismant Al-Kharab: Volume 1 - Roman Period Cartonnage from the Kellis 1 Cemetery. Edited by Colin A. Hope and Gillian E. Bowen. Oxbow Books; 2023.

20. Müller A. Ägyptens schöne Gesichter : die Mumienmasken der Römischen Kaiserzeit und ihre Funktion im Totenritual. Wiesbaden: Reichert Verlag; 2021.

21. Hochscheid H, Russel B. Introduction: New Approaches to Old Crafts. In Hochscheid H & Russel B (eds.) The Value of Making: Theory and Practice in Ancient Craft Production. Brepols Publishers n.v., Turnhout, Belgium; 2021. p. 1–10.

22. Jørgensen, M. Egypt III : Coffins, Mummy Adornments and Mummies from the Third Intermediate, Late, Ptolemaic and the Roman Periods (1080 BC - AD 400): Catalogue: Ny Carlsberg Glyptotek. Ny Carlsberg Glyptotek; 2001.

23. Bagh T. Finds from W.M.F. Petrie's excavations in Egypt in the Ny Carlsberg Glyptotek. (1. ed.). Ny Carlsberg Glyptotek; 2011.

24. Walker S, Bierbrier M. Ancient faces : mummy portraits from Roman Egypt (3. impr.). Publ. for the Trustees of the British Museum by British Museum Press; 1997.

25. Smith M. Dating anthropoid mummy cases from Akhmim: the evidence of the demotic inscriptions. In: Bierbier ML, editor. Portraits and masks

burial customs in Roman Egypt. London: Trustees of the British Museum by British Museum Press; 1997. p. 66–71.

26. Livingstone RJ. Late antique household textiles from the village of Kellis in the Dakhleh Oasis. In de Moor A, Fluck C. Clothing the House: Furnishing Textiles of the 1st Millennium AD from Egypt and Neighbouring Countries: Proceedings of the 5th Conference of the Research Group "Textiles from the Nile Valley" Antwerp 6–7 October 2007. Tielt Belgium: Lannoo.

27. Chauveau M. Egypt in the age of Cleopatra: history and society under the Ptolemies. Ithaca: Cornell University Press; 2000. p. 139–49.

28. Dunand F, Lichtenberg R. Mummies: A voyage through eternity. New York: Discoveries Harry N. Abrams, Inc.; 1994.

29. Venit MS. Visualizing the afterlife in the tombs of Graeco-Roman Egypt. Cambridge: Cambridge University Press; 2017.

30. Bagnall RS, et al. An Oasis City. 1st ed., vol. 6, NYU Press; 2016. https://doi.org/10.18574/9781479818716.

31. Bagnall R, Tallet G, editors. The great oasis of Egypt: the Kharga and Dakhla Oases in Antiquity. Cambridge: Cambridge University Press; 2019. https://doi.org/10.1017/9781108593274.

32. Smelt DH, et al. Investigation of failure in paint films. J Mater Sci. 1979;14(12):2845–52. https://doi.org/10.1007/BF00611464.

33. Salas ME. Evaluating the effectiveness of in-situ non-invasive photophysical characterization methods for distinguishing Indigo from other blue colorants. Los Angeles: University of California; 2020.

34. Altschul SF, Gish W, Miller W, Myers EW, Lipman DJ. Basic local alignment search tool. J Mol Biol. 1990;215(3):403–10. https://doi.org/10.1016/S0022-2836(05)80360-2.

35. van't Hooft PM, Raven MJ, van Rooij EHC, Vogelsang-Eastwood GM. Pharaonic and early Medieval Egyptian textiles. Leiden: Rijksmuseum Van Oudheden; 1994.

36. Aubert MF (in French) Cortopassi R, Nachtergael G, Amoros VA, Détiene P, Pagès-Camagna Le Hô, AS. Funerary portraits from Roman Egypt. Cartonnage, shrouds and wood. Aubert MF (in French) Cortopassi R, Nachtergael G, Amoros VA, Détiene P, Pagès-Camagna Le Hô, AS. Portraits funéraires de l'Egypte romaine. Cartonnages, linceuls et bois. Paris: Editions Khéops-Musée du Louvre; 2008.

37. Granger-Taylor H. Evidence for linen yarn preparation in ancient Egypt. In: Cartwright C, Granger-Taylor H, Quirke. Lahun textile evidence in London in S. Quirke (eds.), Lahun Studies. SIA, Reigate; 1998. p. 103–107.

38. Gleba M, Harris S. The first plant bast fibre technology: identifying splicing in archaeological textiles. Archaeol Anthropol Sci. 2019;11:2329–46. https://doi.org/10.1007/s12520-018-0677-8.

39. Rast-Eicher A. Searching for the earliest wools in Europe. In: K. Grömer/F. Pritchard (eds), Aspects of the Design, Production and Use of Textiles and Clothing from the Bronze Age to the Early Modern Era. NESAT XII. The North European Symposium of Archaeological Textiles, 21th–24thMay 2014 in Hallstatt, Austria. Archaeolingua Main Ser. 33. Budapest; 2015. p. 43–48.

40. Vogelsang-Eastwood G. The production of Linen in Pharaonic Egypt. Leiden; 1992.

41. Letellier-Willemin F. Contribution of the Textiles to the Study of the site of Al-Deir, Kharga Oasis". In C.A. Hope and G.E Bowen (eds.), Proceedings of the Ninth International Dakhleh Oasis Project Conference. Papers presented in honour of Anthony J. Mills. The Oasis Papers 9. Oxford: Oxbow books; 2019. p. 403–409.

42. Fletcher J, Salamone F. An ancient Egyptian wig: construction and reconstruction. Internet Archaeol. 2016. https://doi.org/10.11141/ia.42.6.3.

43. Fletcher J. Hair. In: Nicholson PT, Shaw I, editors. Ancient Egyptian materials and technology. Cambridge: Cambridge University Press; 2000. p. 495–501.

44. Borojevic K, Mountain R. microscopic identification and sourcing of ancient Egyptian plant fibres using longitudinal thin sectioning. Archaeometry. 2010;55:81–112.

45. Kirkinen T, Wright K, Suomela J, Ilves K. Microscopic fibres in soils – the accumulation of textile fibres and animal hairs at the 6th–11th-century CE Kvarnbo Hall settlement site on the Åland Islands, Finland. J Archaeol Sci Rep. 2023;47: 103809.

46. Arizzi A, Cultrone G. Mortars and plasters—how to characterise hydraulic mortars. Archaeol Anthropol Sci. 2021;13:144. https://doi.org/10.1007/s12520-021-01404-2.

Kasso *et al. Heritage Science*   (2024) 12:250

Page 22 of 22

47. Philokyprou M. The earliest use of lime and gypsum mortars in Cyprus. In: Historic Mortars. Springer Netherlands; 2012. pp. 25–35. https://doi.org/10.1007/978-94-007-4635-0_3

48. Lucas A. Mistakes in chemical matters frequently made in archaeology. J Egypt Archaeol. 1924;10(2):128–32.

49. Lucas A. Ancient Egyptian materials & industries. (3rd print). Arnold; 1959.

50. Strudwick H, Dawson J. Death on the Nile: uncovering the afterlife of ancient Egypt. London: D Giles Ltd; 2016. p. 247–51.

51. Gourdin WH, Kingery WD. The beginnings of pyrotechnology: Neolithic and Egyptian lime plaster. J Field Archaeol. 2013;2:133–50.

52. Philokyprou M. The beginnings of pyrotechnology in Cyprus. Int J Archit Herit. 2012;6:172–99.

53. Turco F, Davit P, Chelazzi F, Borghi A, Bombarideri L, Operti L. Characterization of late prehistoric plasters and mortars from Erimi – Laonin Tou Porakou (Limassol, Cyprus). Archaeometry. 2015;58:1–13.

54. Kingery WD, Vandiver PB, Prickett M. The beginnings of pyrotechnology, Part II: production and use of lime and gypsum plaster in the pre-pottery Neolithic near east. J Field Archaeol. 1988;15(2):219–44. https://doi.org/10.2307/530304.

55. Cao W, et al. Recycling of phosphogypsum to prepare gypsum plaster: effect of calcination temperature. J Build Eng. 2022;45: 103511. https://doi.org/10.1016/j.jobe.2021.103511.

56. Akyuz T, et al. Elemental and spectroscopic characterization of plasters from Fatih Mosque-Istanbul (Turkey) by combined Micro-Raman, FTIR and EDXRF techniques. Spectrochimica Acta Part A, Mol Biomol Spectrosc. 2015;149:744–50. https://doi.org/10.1016/j.saa.2015.05.015.

57. Baraldi P, et al. Analytical characterization of Roman plasters of the 'domus Farini' In Modena. Archaeometry. 2006;48(3):481–99. https://doi.org/10.1111/j.1475-4754.2006.00268.x.

58. Anastasiou M, et al. TG-DTA and FTIR analyses of plasters from byzantine monuments in Balkan region: comparative study. J Therm Anal Calorim. 2006;84(1):27–32. https://doi.org/10.1007/s10973-005-7211-9.

59. Chu V, Regev L, Weiner S, Boaretto E. Differentiating between anthropogenic calcite in plaster, ash and natural calcite using infrared spectroscopy: implications in archaeology. J Archaeol Sci. 2008;35(4):905–11. https://doi.org/10.1016/j.jas.2007.06.024.

60. Lucas A, Harris JR. Ancient Egyptian Materials and Industries. 4. ed. rev. and enlarged by J. R. Harris; 1962.

61. Craddock P, Meeks N, Cowell M, Middleton A, Hook D, Ramage A, Geckinli E. The refining of golf in the classical world. In: Williams D, editor. The art of the Greek goldsmith. London: British Museum Press; 1998. p. 111–21.

62. Ogden J. Metals. In: Nicholson PT, Shaw I, editors. Ancient Egyptian materials and technology. Cambridge: Cambridge University Press; 2000. p. 149–76.

63. Verri G. The spatially resolved characterisation of Egyptian blue, Han blue and Han purple by photo-induced luminescence digital imaging. Anal Bioanal Chem. 2009;394:1011–21. https://doi.org/10.1007/s00216-009-2693-0.

64. Scott DA. A review of ancient Egyptian pigments and cosmetics. Stud Conserv. 2016;61(4):185–202. https://doi.org/10.1179/2047058414Y.0000000162.

65. Scott DA, et al. An Egyptian Cartonnage of the Graeco-Roman Period: examination and discoveries. Stud Conserv. 2003;48(1):41–56. https://doi.org/10.1179/sic.2003.48.1.41.

66. Casadio F, Keune K, Noble P, Van Loon A, Hendriks E, Centeno S, Osmond G. Metal soaps in art. Cham, Switzerland: Springer International Publishing; 2019.

67. Rampazzi L. Calcium oxalate films on works of art: a review. J Cult Herit. 2019;40:195–214.

68. Rasmussen KL, Rasmussen BB, Delbey T, et al. Analyses of the brown stain on the Parthenon Centaur head in Denmark. Herit Sci. 2024;12:18. https://doi.org/10.1186/s40494-023-01126-9.

69. Alunno-Rossetti V, Marabelli M. Analyses of the patinas of a gilded horse of St Mark's Basilica in Venice: corrosion mechanisms and conservation problems. Stud Conserv. 1976;21(4):161–70.

70. Nevin A, Melia JL, Osticioli I, Gautier G, Colombini MP. The identification of copper oxalates in a 16th century Cypriot exterior wall painting using micro FTIR, micro Raman spectroscopy and Gas Chromatography-Mass Spectrometry. J Cult Herit. 2008;9(2):154–61.

71. Zoppi A, Lofrumento C, Mendes NFC, Castellucci EM. Metal oxalates in paints: a Raman investigation on the relative reactivities of different pigments to oxalic acid solutions. Anal Bioanal Chem. 2010;397:841–9.

72. Cosentino A. Identification of pigments by multispectral imaging; a flow-chart method. Herit Sci. 2014;2:8. https://doi.org/10.1186/2050-7445-2-8.

73. Corcoran LH, Svodoba M. Herakleides: a portrait mummy from Roman Egypt. Los Angeles: J Paul Getty Museum; 2010.

74. Eastaugh N. Pigment compendium: a dictionary and optical microscopy of historical pigments. Oxford: Butterworth-Heinemann; 2004.

75. Skovmøller A, Brøns C, Sargent ML. Egyptian blue: modern myths, ancient realities. J Roman Archaeol. 2016;29:371–87. https://doi.org/10.1017/S1047759400072184.

76. Nicola M, Gobetto R, Masic A. Egyptian blue, Chinese blue, and related two-dimensional silicates: from antiquity to future technologies. Part A: general properties and historical uses. Rendiconti Lincei Scienze Fisiche e Naturali. 2023;34:369–413. https://doi.org/10.1007/s12210-023-01153-5.

77. Dyer J, Tamburini D, Sotiropoulou S. The identification of lac as a pigment in ancient Greek polychromy - The case of a Hellenistic oinochoe from Canosa di Puglia. Dyes Pigm. 2018;149:122–32. https://doi.org/10.1016/j.dyepig.2017.09.062.

78. Svodoba M, Cartwright C, editors. Mummy portraits of Roman Egypt: emerging research from the APPEAR Project. Los Angeles: J. Paul Getty Museum; 2020.

79. Daniels V, Stacey R, Middleton A. The blackening of paint containing Egyptian Blue. Stud Conserv. 2004;49(4):217–30. https://doi.org/10.1179/sic.2004.49.4.217.

80. Mills J, White R. The organic chemistry of museum objects. 2nd ed. Oxford: Butterworth-Heinemann; 1994.

81. Glickman M. Gum technology in the food industry. London: Academic Press; 1969.

82. Newman R, Serpico M. Adhesives and binder. In: Nicholson PT, Shaw I, editors. Ancient Egyptian materials and technology. Cambridge: Cambridge University Press; 2000. p. 478–94.

83. Granzotto C, Arslanoglu J. Revealing the Binding medium of a Roman Egyptian painted mummy shroud. J Cult Herit. 2017;27:170–4. https://doi.org/10.1016/j.culher.2017.04.005.

84. Partridge R. Transport in Ancient Egypt. Rubicon; 1996.

85. Serpico M, White R. Oil, fat and wax. In: Nicholson PT, Shaw I, editors. Ancient Egyptian materials and technology. Cambridge: Cambridge University Press; 2000. p. 390–429.

86. Krzyszkowska O, Morkot R. Ivory and related materials. In: Nicholson PT, Shaw I, editors. Ancient Egyptian materials and technology. Cambridge: Cambridge University Press; 2000. p. 320–31.

Publisher's Note